AIAA JOURNAL
Vol. 40, No. 6, June 2002

Investigation of Gaseous Acoustic Damping Rates by Transient Grating Spectroscopy

Yuanyuan Li* and William L. Roberts†
North Carolina State University, Raleigh, North Carolina 27695-7910
and
Michael S. Brown‡
Innovative Scientific Solutions, Inc., Dayton, Ohio 45440-3638

An investigation of acoustic damping rates in a pressurized gaseous medium by analyzing the temporal behavior of laser-induced gratings is reported. Experiments were performed in various nonresonant gas samples as a function of pressure and grating spacing. Acoustic damping rates were determined through model fits to the acquired signals. The results were compared with theoretical calculations using both classical acoustic damping rates and a more comprehensive model that includes rotational and vibrational energy transfer mechanisms. The relationships between the measured acoustic damping rate and molecular structure and pressure and grating spacing are discussed. The utility of exploiting the temporal signature from laser-induced gratings to determine acoustic damping rates in high-pressure gases is identified.

Nomenclature

c_p	=	heat capacity at constant pressure
c_{rot}	=	heat capacity of rotational modes
c_s	=	local speed of sound
c_v	=	heat capacity at constant volume
c_{vib}	=	heat capacity of vibrational modes
D_{th}	=	thermal diffusivity
f	=	acoustic frequency
G	=	geometric factor
I	=	signal intensity
M	=	molecular weight
P	=	pressure
$\boldsymbol{q}$	=	grating wave vector, $2\pi/\Lambda$
R	=	gas constant
T	=	fluid temperature
t	=	time
Z	=	collision number
β	=	damping factor due to energy transfer
Γ	=	acoustic damping coefficient
γ	=	specific heat ratio
Δn	=	local modulation in index of refraction
η	=	scattering efficiency of laser-induced grating
θ	=	full angle between beams
κ	=	thermal conductivity
Λ	=	grating spacing
λ	=	laser wavelength
μ	=	dynamic viscosity
ρ	=	fluid density
τ_{rot}	=	rotational relaxation time
τ_{vib}	=	vibrational relaxation time

Presented as Paper 2001-0849 at the AIAA 39th Aerospace Sciences Meeting, Reno, NV, 8–11 January 2001; received 5 March 2001; revision received 21 September 2001; accepted for publication 19 October 2001.

*Research Assistant, Department of Mechanical and Aerospace Engineering. Member AIAA.
†Associate Professor, Department of Mechanical and Aerospace Engineering; wlrobert@eos.ncsu.edu. Member AIAA.
‡Research Physicist, 2766 Indian Ripple Road. Member AIAA.

Introduction

THE transient grating spectroscopy (TGS) technique relies on the first-order Bragg scattering of a probe laser beam from a dynamic grating generated by a pair of crossed, pulsed pump beams. The amplitude of the signal scales quadratically with pressure and pump beam intensity and linearly with probe beam intensity. The temporal behavior of the signal is a function of the local temperature and transport properties. The oscillation frequency of the signal amplitude is a function of the local sound speed from which the local temperature can be extracted. The decay of the signal amplitude is due to thermal diffusion, molecular diffusion, viscous dissipation, and molecular energy transfer. Historically, laser-induced grating techniques have been developed to explore many time-dependent phenomena in liquids and solids.[1] Only recently, investigators have applied the TGS technique to studies in the gaseous phase. Since the observation of the acoustic response induced by a nonresonant laser in the gaseous phase by Govoni et al.,[2] different groups have analytically described the temporal behavior of the TGS signal[3,4] for both resonant and nonresonant laser induction. The TGS technique has been used to measure sound velocity,[5,6] temperature,[7–9] thermal diffusivity,[10] and fluid flow velocity[11,12] in a number of laboratories.

Soon after the laser-induced grating signal was observed and its time dependent behavior was analyzed, it was proposed as a potential thermometer to be applied in combustion environments because of its simplicity. The oscillation frequency of the TGS signal is proportional to the local speed of sound, which in turn is a simple function of the local temperature under ideal gas assumptions. However, the combustion products are composed of many different species, and therefore, determination of the local temperature requires knowledge of the local average molecular mass M and the ratio of specific heats γ. For overall lean hydrocarbon–air diffusion flames, the major species will be nitrogen, water, carbon dioxide, and oxygen, with lesser amounts of carbon monoxide. M and γ are determined by these major species and are relatively insensitive to the dozens of minor species that may be present.

In the present paper, we report measurements of the acoustic damping rate in high-pressure gaseous environments by analysis of the temporal decay of nonresonantly induced TGS signals. This damping rate is determined by the molecular composition of the test gas because it reflects the viscosity, thermal diffusivity, and collisional energy transfer behavior of the constituent gases. The measurements reported here were conducted on pure gas samples. Our aim was to demonstrate the ability of TGS to measure acoustic damping rates at elevated pressure. Strong differences in the acoustic damping rate in pure atomic, diatomic, triatomic, and polyatomic gases suggest the possibility of detecting the relative mixture

fractions of the major species in a gas mixture composed primarily of simple species.

Theory

TGS

If two laser beams with parallel, linear polarization are spatially and temporally overlapped, an intensity grating will be formed in the medium with a grating spacing Λ given by

$$\Lambda = \lambda/2\sin(\theta/2) \tag{1}$$

The wavelength of the grating-inducing beams is given by λ, whereas the full angle between the beams is θ. Through various physical mechanisms, the light intensity grating produces a modulation in the local index of refraction Δn (Ref. 1). Typically, two of these processes are important: First, A high-intensity nonresonant light field will modulate the local fluid density through the process of electrostriction.[13] During electrostriction, the electric field gradient partially polarizes the molecules, impulsively accelerating them into the region of high field intensity. Not all molecules have the same susceptibility to this polarization, as measured by the electrostrictive coefficient. This molecular movement modulates the local density and, hence, the local index of refraction. Second, certain resonant species in the target medium will absorb some of the incident light energy and then modulate the local density through the process of thermalization. During thermalization, a target molecular species optically absorbs energy through an allowable rovibronic transition. (Electronic transitions are accessed with the visible pump sources used in the work.) Via inelastic collisions, the absorbed energy in the excited species is transferred to the surrounding gas, locally heating it and producing a thermal grating and concomitant modulation of the local index of refraction. The hydrodynamic response of the gas to both electrostriction and thermalization is to produce two counterpropagating acoustic waves and a nonpropagating but diffusing entropy or thermal wave. The alternating constructive and destructive interference of the two sound waves produces a standing sound wave and makes the local index of refraction oscillate at a frequency (the Brillouin frequency) solely determined by the grating spacing and the local speed of sound. The pulsed pump beams, which form the grating (ideally delta functions in time), have a pulse width of approximately 10 ns in these experiments, whereas the probe beam operates in a continuous wave mode. After the grating-inducing pulses have passed through the sample volume, the grating structures themselves will be washed out in time due to dissipation of both acoustic and thermal waves.

The optical grating can be efficiently read out by the probe beam with wavelength λ_{pr} under the Bragg scattering (coherent scattering) condition expressed by the relation

$$\lambda_{\text{probe}}/\sin(\theta_{\text{probe}}/2) = \lambda_{\text{pump}}/\sin(\theta_{\text{pump}}/2) \tag{2}$$

The scattering efficiency η of laser-induced grating is[14]

$$\eta = I_{\text{signal}}/I_{\text{probe}} = G\sin^2[\pi(L/\lambda_{\text{probe}})\Delta n] \tag{3}$$

The geometric factor G includes the spatial profiles and spatial overlap of the incident beams. Δn is the perturbation of the index of refraction and L is the length of the grating. For relatively weak diffraction, Eq. (3) can be approximated as

$$\eta \approx G[\pi(L/\lambda_{\text{probe}})\Delta n]^2 \tag{4}$$

Expanding the index-of-refraction perturbation in terms of two fluid variables whose fluctuations are statistically independent, namely, density and temperature, we have

$$\Delta n = \left(\frac{\partial n}{\partial \rho}\right)_T \Delta\rho + \left(\frac{\partial n}{\partial T}\right)_\rho \Delta T \tag{5}$$

The second term in Eq. (5) is quite small in gases and can be neglected compared to the first.[3] Therefore, the relation between scattering efficiency and the local density perturbation can be approximately expressed as

$$\eta \approx G\left[\pi \frac{L}{\lambda_{\text{probe}}}\left(\frac{\partial n}{\partial \rho}\right)\Delta\rho\right]^2 \tag{6}$$

The TGS signal I_{signal} is, thus, proportional to $\Delta\rho^2$. As indicated earlier, the density variation caused by laser-induced gratings is composed of two counterpropagating acoustic waves and a nonpropagating, but diffusing, entropy or thermal wave. Therefore, the total TGS signal appears as an exponentially damped oscillation. The exponential decay of the envelope provides a measure of the acoustic damping rate and thermal diffusivity. For excitation by an infinitely short laser pulse at the initial moment $t = 0$, the signal will be given approximately at $t > 0$ as[5,6]

$$I_{\text{signal}}(t) \propto \left\{A\exp\left(-D_{\text{th}}q^2t\right) + B\exp(-\Gamma q^2 t)\cos(c_s\boldsymbol{q}t + \phi)^2\right\} \tag{7}$$

The grating wave vector $\boldsymbol{q}$ is defined as $\boldsymbol{q} = 2\pi/\Lambda$. The coefficients A and B and phase angle ϕ are simply used as fitting parameters. The ratio of A to B determines the relative amounts of electrostriction and thermalization present in the signal. The parameter ϕ is useful in fitting noisy data in which there is ambiguity in setting the zero point on the timeline. Note that Eq. (7) is an approximation in the sense that it presumes an infinitely fast thermalization rate and a pump laser with an infinitely narrow pulse width, as well as pump and probe beams with plane wave fronts of infinite extent.

From Eq. (7), we see that the TGS signal has a gradual decay due to diffusion and acoustic damping with an oscillation superimposed on it. From the gradual decay rate, the local thermal diffusivity can be extracted when thermal gratings are excited.[10] The decreasing magnitude of the oscillation part in the TGS signal represents the absorption of the acoustic wave intensity.

Classical Acoustic Damping

In a classical view, the energy of the sound wave is dissipated due to both internal friction and heat conduction; therefore, the damping rate of the amplitude of an acoustic wave is a function of the transport properties of viscosity and thermal conductivity. The classical acoustic damping coefficient in a gas can be expressed as

$$\Gamma_c = (1/2\rho_0)\left[\tfrac{4}{3}\mu + (\gamma - 1)(\kappa/c_p)\right] \tag{8}$$

where ρ_0 is the gas density. By curve fitting the TGS signal with Eq. (7), the acoustic damping coefficient may be extracted.

Acoustic Damping in Real Gases

The classical acoustic damping coefficient works well for atomic species, as will be shown. However, for molecules, vibrational and rotational energy transfer must be accounted for, in the attenuation of acoustic modes.[15–18] A rigorous mathematical discussion is not presented, just the salient points. First note that, because $\boldsymbol{q} = 2\pi/\Lambda$ and $\Lambda f = c_s$, $\boldsymbol{q}^2$ can be written as ω^2/c_s^2, where $\omega = 2\pi f$. The damping factor in the second term of Eq. (7) is then rewritten as

$$\exp\left[\left(-\omega^2/c_s^2\right)\Gamma_c t\right] \tag{9}$$

As already noted, Γ_c includes viscous and diffusive damping. Damping due to energy transfer and damping due to viscosity and diffusion effects are additive.[16–18] For a single component gas, Eq. (9) can be rewritten as

$$\exp\left[-\beta t - \left(\omega^2/c_s^2\right)\Gamma_c t\right] \tag{10}$$

where β is a function of molecular parameters and the local thermodynamic state. For simplicity we report and discuss the ratio

$$\frac{\Gamma_m}{\Gamma_c} = \frac{\beta + \left(\omega^2/c_s^2\right)\Gamma_c}{\left(\omega^2/c_s^2\right)\Gamma_c} \tag{11}$$

where Γ_m is the measured damping coefficient. Various authors have discussed analytical expressions for β. Summaries of this work may be found in Refs. 15–18. These discussions are aimed at elucidating the frequency and temperature dependence of the acoustic attenuation due to energy transfer (relaxation), and the pressure dependence of the attenuation is not explicitly developed. Inclusion of

translation to rotation energy transfer at 1 atm leads to the following approximate expression[18]:

$$\Gamma_m/\Gamma_c = 1 + X(c_{\text{rot}}/R)Z \tag{12a}$$

where

$$X = \tfrac{3}{5}\left(R^2/c_v c_p\right)\{\gamma/[1 + (3/16\gamma)(9\gamma - 5)(\gamma - 1)]\} \tag{12b}$$

where Z denotes the collision number given by the ratio of the rotational relaxation time to the time between collisions. Equation (12) assumes that $\omega\tau_{\text{rot}} \ll 1$. The inclusion of translation to vibration energy transfer requires the addition of a third term to the right-hand side of Eq. (12), namely,

$$\pi r\left\{\omega\tau_{\text{vib}}/\left[1 + \omega^2\tau_{\text{vib}}^2(1 - r)\right]/\Gamma_c\right\} \tag{13a}$$

where

$$r = c_{\text{vib}}R/c_v c_p \tag{13b}$$

The term is valid at all values of $\omega\tau_{\text{vib}}$.

Experiments

The optical setup for the TGS experiments presented here is shown schematically in Fig. 1. The frequency-doubled output of a Q-switched, Nd:YAG laser was used to write the gratings. A beam splitter divided the Nd:YAG beams into two pump beams of equal energy (10 Hz; 50 ~ 150 mJ per pump beam). The 514-nm probe beam was provided by an Ar ion laser to read out the gratings. During alignment of the detector, ~4% of the probe beam is split off to trace out the path of the actual TGS signal beam. The four laser beams were directed to the investigation point inside the high-pressure gas cell while satisfying phase matching conditions. The signal beam is directed by a mirror through spatial and spectral filters and then onto a photomultiplier tube (PMT). The PMT was connected to a digital oscilloscope to acquire the TGS signals. The signals are typically acquired and saved into the computer for offline analysis. The high-pressure gas cell, 12.7 cm in diameter, was built to operate at pressures up to 35 atm. To provide optical access, two 25.4-mm-thick BK-7 windows are mounted along the optical path.

In the previously reported TGS thermometry experiments,[7] the pump beams and the probe beam were crossed at the investigation point using a simple focusing lens. Focusing of the pump beams provides sufficient intensity to generate gratings in high-temperature (modest density) conditions. In the present work, unfocused laser beams were used to measure the transport properties. With the exception of the reduced laser intensity in the crossover region, the probe volume generated by unfocused pump beams is much larger than that formed by focused pump beams. With focused pump beams, the probe volume is a long, thin ellipsoid about

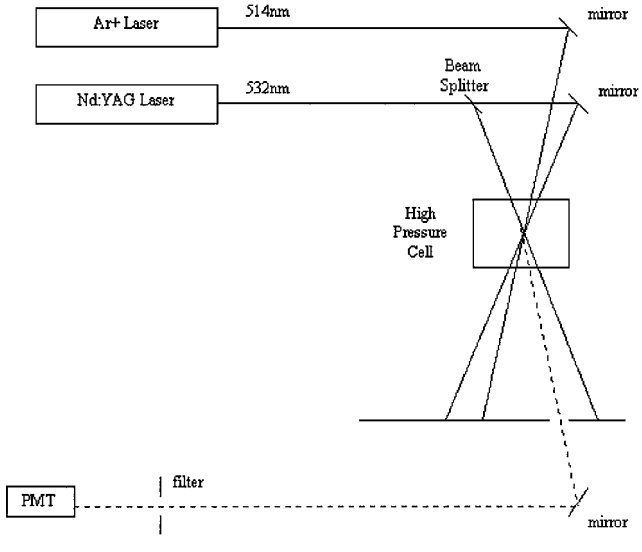

Fig. 1 Schematic of the TGS optical setup.

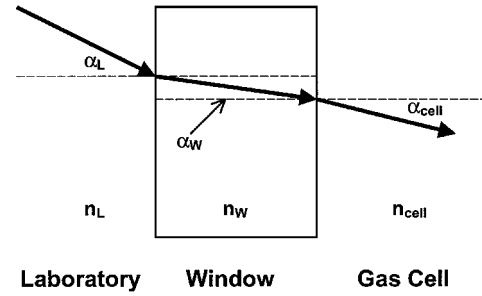

Fig. 2 Schematic of the path of one of the pump beams as it passes from the laboratory through the window into high-pressure gas cell.

a few hundred micrometers in diameter (at the widest point) and several millimeters long. Using unfocused pump beams, the diameter of the probe volume is ~8 mm in the present TGS experiments. When the probe volume diameter is small, the effect of the sound waves propagating out the probe volume gives a contribution to the grating reflectance decay rate. Therefore, one must provide a correction when extracting the acoustic damping rate from the decay of the oscillating part of the TGS signal.[4] Because the environment inside the high-pressure gas cell is homogeneous, we used an unfocused beam setup. When better spatial resolution is desired, such as in small samples or inhomogeneous environments, focused pump beams should be used and attention should be paid to the effect of the sound waves propagating out of the probe volume.

Once the initial alignment was established, the high-pressure gas cell was filled with either pressurized air or CO_2. The electrostrictive response from this gas sample is used to optimize the TGS signal. Additionally, the actual grating spacing Λ was accurately determined through signal analysis of the oscillation frequency. The index of refraction inside the high-pressure gas cell will change with different gas samples and pressures. As shown in Fig. 2, the wavelengths of the pump beams inside and outside the high-pressure gas cell are related via

$$\lambda_{\text{cell}} = (\lambda_L/n_{\text{cell}})n_L \tag{14}$$

In Fig. 2, the angles and indices of refraction needed for Snell's law are β_i and n_i, respectively. From Snell's law,

$$n_L \sin(\alpha_L) = n_W \sin(\alpha_W) = n_{\text{cell}} \sin(\alpha_{\text{cell}}) \tag{15}$$

where α is the half-angle between two pump beams. Combining Eqs. (14) and (15), we can rewrite Eq. (1) as

$$\Lambda = \frac{\lambda_{\text{cell}}}{2\sin(\alpha_{\text{cell}})} = \frac{\lambda_L n_L}{2n_{\text{cell}}\sin(\alpha_{\text{cell}})} = \frac{\lambda_L}{2\sin(\alpha_L)} \tag{16}$$

From Eq. (16), we see that the grating spacing Λ is determined entirely by the crossing angle and wavelength of the pump beams. Therefore, we can measure the value of the grating spacing using the signal of the alignment gas sample, and then use this value of Λ to interpret all other TGS signals. In all reported measurements, dry, high-purity (>99.99% pure) gases were used. When changing gas samples inside the gas cell, the gas cell was first filled with new gases, then the cell was evacuated by a vacuum pump. This procedure was repeated three times to make sure that there was very little residue of previously tested gases. After evacuation, the cell was filled to the desired pressure with the new test gas.

Results and Discussion

The TGS experiments were performed with various neat gas samples (Ar, N_2, CO_2, CH_4, etc.) over a range of pressures (from 1 to 25 atm). Examples of signals from atomic, diatomic, triatomic, and higher-order polyatomic species of combustion interest are shown in Fig. 3 The grating spacing $\Lambda \cong 22\ \mu$m. All signals shown are due to the nonresonant electrostrictive response.

To acquire the information of acoustic damping rate, the TGS signals were curve fitted with the expression in Eq. (7). Commercial software (KaleidaGraph®), which employs the Levenberg–Marquardt algorithm, was utilized in the nonlinear least-squares fit

of the TGS signals. A typical example is shown in Fig. 4. The TGS signal was acquired from CH_4 at 6.4 atm. For the extracted TGS signal frequency, the curve-fitting error is usually very small, less than 0.1%; for the TGS signal damping rate, the curve-fitting error is usually less than 5%, for example, 1.2% for the signal shown in Fig. 4. Table 1 presents some measured results of the acoustic damping rate Γ_m along with values of classical acoustic damping coefficients Γ_c calculated using Eq. (8). In Table 1, only Ar exhibits a measured acoustic damping rate close to the calculated result from classical theory. For the other diatomic and polyatomic gases, the measured acoustic damping rate is higher than the calculated classical acoustic damping rate reflecting attenuation due to energy transfer and illustrating the utility of TGS in determining these acoustic dissipation rates for molecular species. The most important source of the increased attenuation is the collisional transfer of translational energy to rotational and/or vibrational energy modes of the constituent molecules. Whereas translation and rotation modes typically equilibrate quickly, vibrational energy transfer is much slower and, for small molecules, is efficient only at elevated temperatures. The rate of collisional transfer of translational energy to rotational and/or vibrational energy modes is determined by the collision rate between molecules, which is a function of the temperature and pressure, as well as the rotational and/or vibrational energy modes distribution, which is determined by the molecular structure. The absence of these

Table 1 Acoustic damping rates at 6.4 atm, 20° C[a]

Species	Γ_m, 10^{-6} m^2/s[b]	Γ_c, 10^{-6} m^2/s[c]
Ar	2.32	2.34
N_2	4.90	2.31
CO_2	3.45	1.10
CH_4	6.17	2.12
C_2H_4	18.12	1.16

[a]Grating spacing $\Lambda \cong 22$ μm.
[b]Values from measured TGS signals.
[c]Values calculated from Eq. (8).

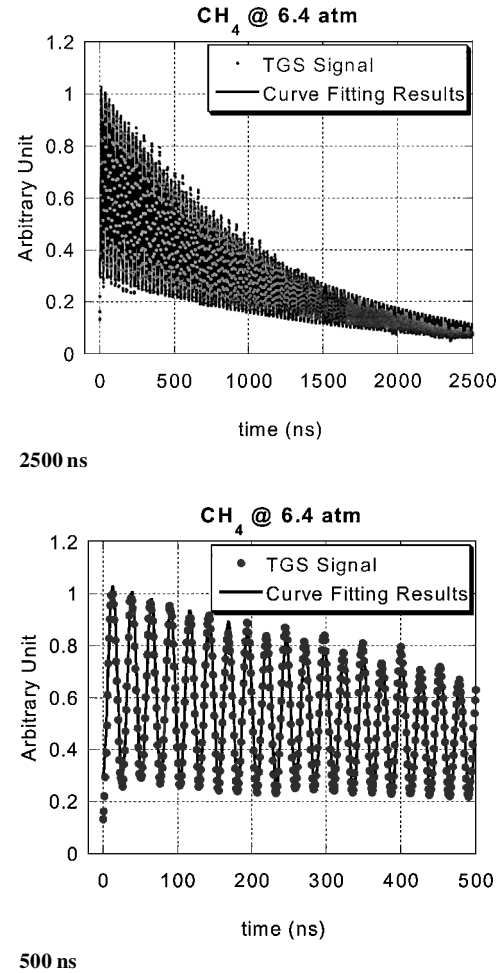

Fig. 4 Sample TGS signal with best fit over two temporal ranges.

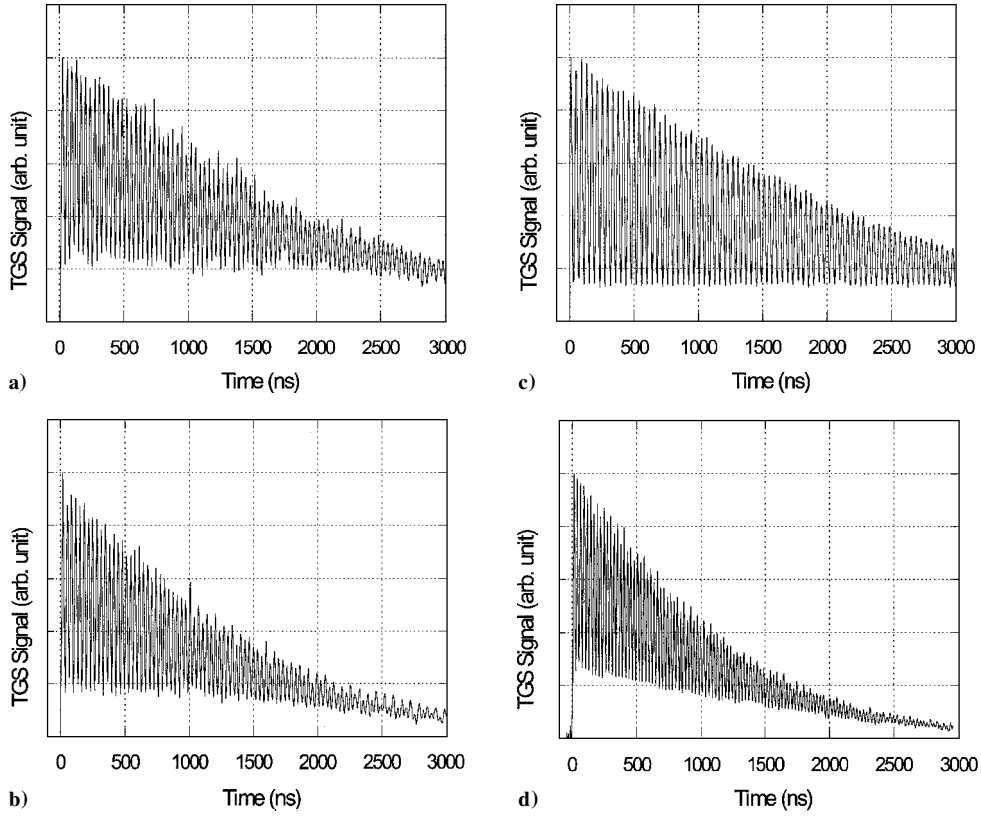

Fig. 3 TGS signal (averaged over 64 laser shots) samples: a) Ar, b) N_2, c) CO_2, and d) CH_4 at 6.4 psig.

rotational/vibrational modes in atomic species explains why acoustic damping in Ar is fairly well predicted by the classical theory.

In Fig. 5, the measured acoustic damping rate ratio Γ_m/Γ_c is plotted, for gas samples of Ar, N_2, and CO_2 as a function of pressure. As seen, this ratio increases with pressure for the molecular species, due to the increase in relative importance of molecular energy transfer with increasing pressure. Although both viscosity and thermal conductivity increase with increasing pressure for pure gases, the increase is quite small and not enough to account for the large damping rate increase.[19] The reason for this larger acoustic damping rate is that, at higher pressure, the excess translational energy is converted to rotational and/or vibrational energy faster due to the greater collisional frequency.

For atomic gases such as Ar and He, the measured acoustic damping rate from the TGS signal is essentially equal to the calculated classical acoustic damping rate over an extended pressure range. For N_2, previous studies[20] have shown $\Gamma_m/\Gamma_c = 1.4$ at atmospheric pressure, which is very close to the results shown in Fig. 5. This ratio increases with increasing pressure due to the relative increase in the importance of translational to rotational energy transfer. For CO_2, both rotational modes and the lowest frequency vibrational mode receive energy from the excess translational energy, and the damping ratio exceeds that of N_2. For molecules with more complicated structure, such as C_2H_4, the acoustic damping rate ratio not only is much higher because of the greater number of available internal energy modes, but its dependence on pressure becomes nonlinear. As the number of low-energy (bending) modes increases, the damping rate will increase because these low-energy modes are less likely to be frozen. Molecules with relatively simple structure, such as N_2 and CO_2, exhibit acoustic damping ratio changes that depend linearly on pressure increase as shown in Fig. 5. The acoustic damping rate ratios of C_2H_4 and N_2 are shown as a function of pressure in Fig. 6.

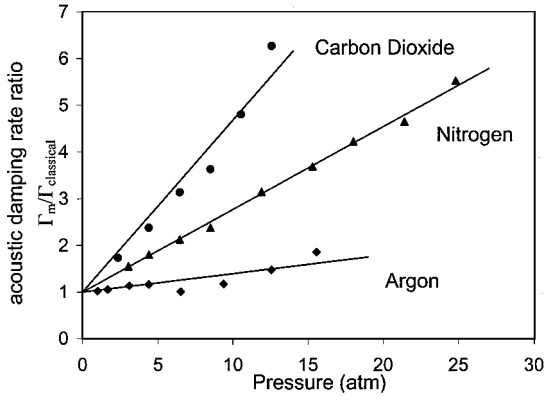

Fig. 5 Acoustic damping rate ratio Γ_m/Γ_c vs pressure P for Ar, N_2, and CO_2; grating spacing $\Lambda \cong 22$ μm.

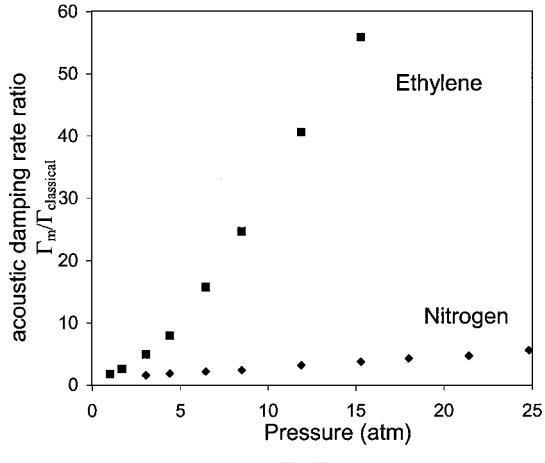

Fig. 6 Acoustic damping rate ratio Γ_m/Γ_c vs pressure for N_2 and C_2H_4; grating spacing $\Lambda \cong 22$ μm.

Table 2 presents the acoustic damping rate ratios of three diatomic gases, N_2, O_2, and CO, at different pressures. We can see that the acoustic damping rate ratio for these diatomic gases are very similar at fixed pressure, and the changes with pressure are similar as well. The similarity is because the translational/rotational energy transfer efficiency is similar for all three gases, as well as their molecular weights and, hence, relative velocities. Interestingly, CH_4 has an acoustic damping ratio similar to that of CO_2 at room temperature, as shown in Fig. 7.

To model the effect of increasing pressure on the damping rate ratio, we augmented the model in Eqs. (12) and (13) to include a prefactor, linear in pressure, namely, $P/2$. As already noted, Eqs. (12) and (13) were not developed to handle explicit pressure dependence studies. We have found in our work that multiplying the second term on the right-hand side of Eq. (12a) and the single term in Eq. (13a) by $P/2$ (atm) yields good results in comparisons with experiment,

Table 2 Acoustic damping rate ratio Γ_m/Γ_c of diatomic gases at different pressures[a]

Pressure, atm	N_2	O_2	CO
4.4	1.8	1.57	1.85
7.8	2.25	1.92	2.15
11.2	2.92	2.68	2.88
14.6	3.55	3.19	3.5
18	4.23	3.99	4.37

[a]Grating spacing $\Lambda \cong 22$ μm.

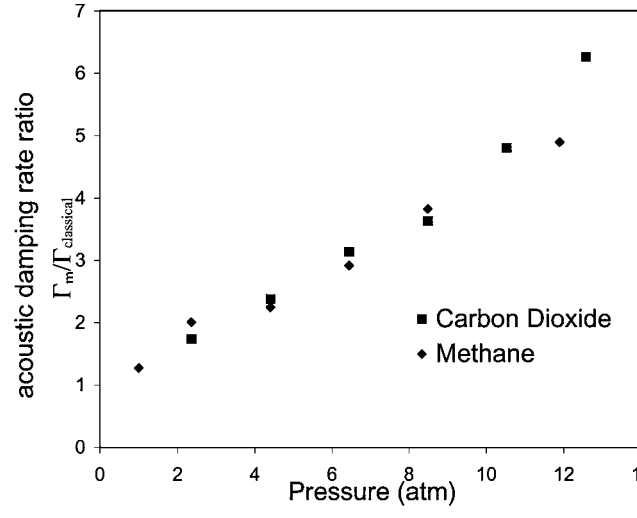

Fig. 7 Acoustic damping rate ratio Γ_m/Γ_c vs pressure for CO_2 and CH_4; grating spacing $\Lambda \cong 22$ μm.

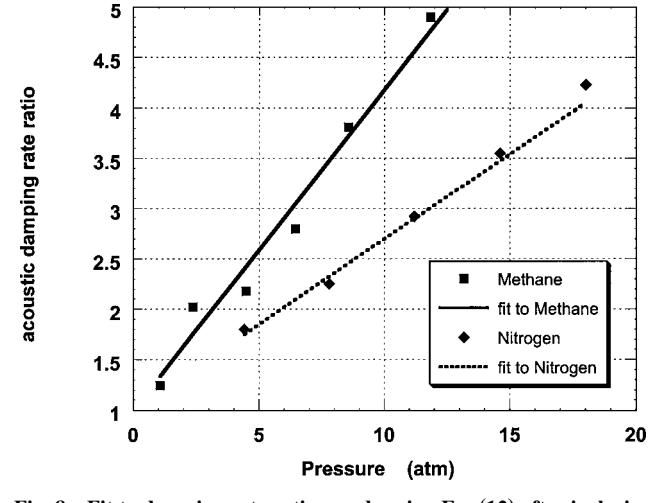

Fig. 8 Fit to damping rate ratios made using Eq. (12) after inclusion of the $P/2$ prefactor. Z was used as the fit parameter.

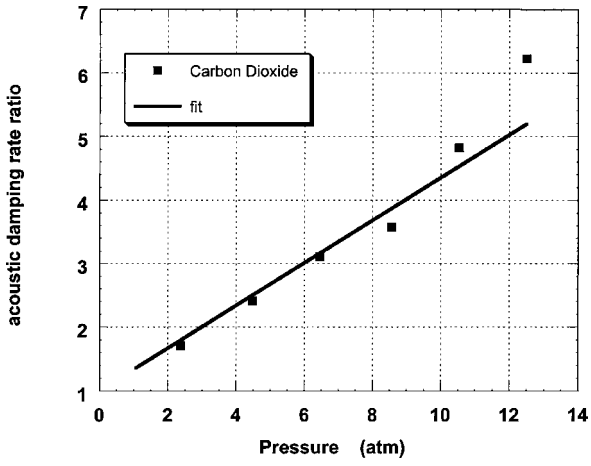

Fig. 9 Best fit to CO_2 damping rate ratio made with Eqs. (12) and (13) and inclusion of the *P*/2 prefactor.

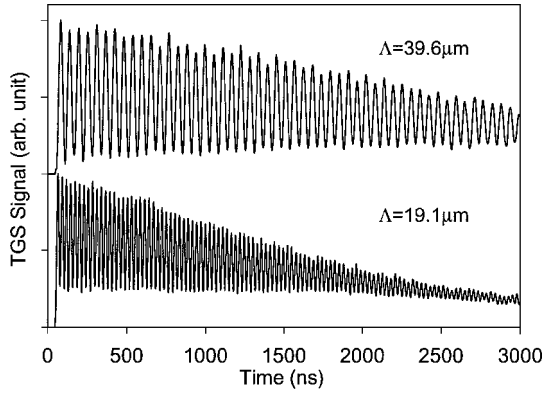

N_2 at 18 atm

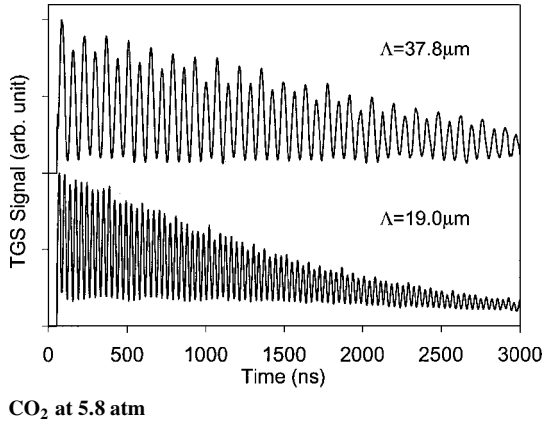

CO_2 at 5.8 atm

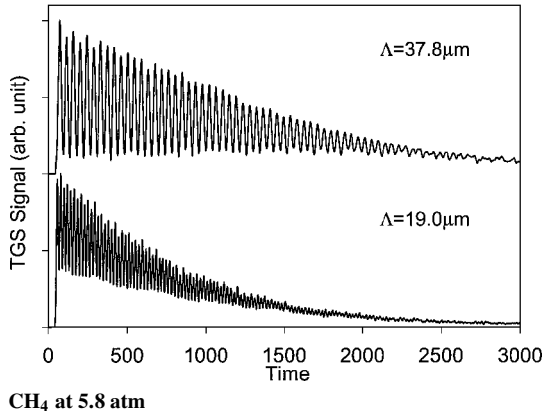

CH_4 at 5.8 atm

Fig. 10 TGS signals (averaged over 64 laser shots) at different grating spacings.

as shown in Figs. 8 and 9. The fits were made to the N_2, CH_4, and CO_2 data by varying the collision number Z. We find that $Z = 5$, 15, and 16 for N_2, CH_4, and CO_2, respectively. These values are in excellent agreement (within experimental error) with published literature values.[15] The fits to the nitrogen and methane data were made using only the modified form of Eq. (12), which incorporates rotational energy transfer. The fit to the carbon dioxide data was made using Eqs. (12) and (13) and the published room temperature vibrational relaxation time of $\tau_{vib} = 6\ \mu s$ (Ref. 15).

Note that each of the damping terms, classical ($\Gamma_c \omega^2 / c_s^2$), rotational ($\omega Z X c_{rot}/R$), and vibrational [$\omega$ times Eq. (13)] relaxation, vary as ω or ω^2, which is equivalent to varying as $1/\Lambda$ or $1/\Lambda^2$. Therefore, changing the grating spacing is the same as changing the acoustic frequency. Off-resonance, acoustic attenuation often increases with frequency, and this is observed in our TGS measurements as shown in Fig. 10. In principle, the grating spacing could be varied continuously to find local maxima in the attenuation, which is equivalent to finding the effective relaxation time.[15] Such maxima serve to identify the absorbing species.

Summary

The experimental TGS acoustic damping rate data presented is characterized by three trends: 1) The acoustic damping ratio increases with increasing molecular complexity. 2) The damping ratio increases with increasing pressure. 3) Acoustic damping increases with increasing acoustic frequency. It has been demonstrated that the acoustic damping rates of pure gases at different conditions can be investigated through model fits of TGS signals. The Ar result is in good agreement with the simple theoretical calculations for a monatomic gas, as expected. For polyatomic gases, the decay rates are faster than those estimated from the simple acoustic theory. This is caused by the collisional transfer of translational energy to rotational/vibrational energy. Higher pressure causes the acoustic wave to decay faster because of the higher collisional rate between molecules. Increased molecular complexity leads to increased attenuation due to the increased number of internal modes that can receive excess translational energy. For molecules with similar rotational and vibrational modes (number and characteristic energies) and masses, the contribution of collisional energy transfer to the acoustic damping rate is similar at fixed pressure.

Based on the work presented here, we anticipate the ability to distinguish between types of gas mixtures. Knowledge of the pressure combined with a measurement of Γ_m at a carefully selected frequency ω should permit discrimination between exhaust gases and unburned gases, for example. Typically, hydrocarbon fuels will be polyatomic, products will be triatomic (water and carbon dioxide), and air/oxidizer will be diatomic. With the ability to measure acoustic damping rates with TGS, it may be possible to discern information regarding the state of the combustion process. Future work will examine this possibility.

Acknowledgment

We thank James Gord of the U.S. Air Force Research Laboratory at Wright–Patterson Air Force Base for his support and assistance with equipment.

References

[1]Eichler, H. J., Gunter, P., and Pohl, D. W., *Laser-Induced Dynamic Gratings*, Springer-Verlag, Berlin, 1986.

[2]Govoni, D. E., Booze, J. A., Sinha, A., and Crim, F. F., "The Non-Resonant Signal in Laser-Induced Grating Spectroscopy of Gases," *Chemical Physics Letters*, Vol. 216, No. 3, 1993, pp. 525–529.

[3]Paul, P. H., Farrow, R. L., and Daneby, P. M., "Gas-Phase Thermal-Grating Contributions to Four-Wave Mixing," *Journal of the Optical Society of America B*, Vol. 12, No. 3, 1995, pp. 384–392.

[4]Cummings, E. B., Leyva, I. A., and Hornung, H. G., "Laser-Induced Thermal Acoustics (LITA) Signals from Finite Beams," *Applied Optics*, Vol. 34, No. 18, 1995, pp. 3290–3302.

[5]Cummings, E. B., "Laser-Induced Thermal Acoustics, Simple Accurate Gas Measurements," *Optics Letters*, Vol. 19, No. 17, 1994, pp. 1361–1363.

[6]Hubschmid, W., Bombach, R., Hemmerling, B., and Stampanoni-Panariello, A., "Sound-Velocity Measurements in Gases by Laser-Induced Electrostrictive Gratings," *Applied Physics B*, Vol. 62, 1996, pp. 103–107.

[7]Brown, M. S., and Roberts, W. L., "Single-Point Thermometry in High-Pressure, Sooting, Premixed Combustion Environment," *Journal of Propulsion and Power*, Vol. 15, No. 1, 1999, pp. 119–127.

[8]Hemmerling, B., Hubschmid, W., and Stampanoni-Panariello, A., "Temperature and Mixture Fraction Measurements in Gases by Laser Induced Electrostrictive Gratings," *Twenty-Seventh Symposium (International) on Combustion*, Combustion Inst., Pittsburgh, PA, 1998, pp. 69–75.

[9]Hart, R. C., Balla, R. J., and Herring, G. C., "Nonresonant Referenced Laser-Induced Thermal Acoustic Thermometry in Air," *Applied Optics*, Vol. 38, No. 3, 1999, pp. 577–584.

[10]Cummings, E. B., Hornung, H. G., Brown, M. S., and DeBarber, P. A., "Measurement of Gas-Phase Sound Speed and Thermal Diffusivity over a Broad Pressure Range Using Laser-Induced Thermal Acoustics," *Optics Letters*, Vol. 20, No. 14, 1995, pp. 1577–1579.

[11]Hemmerling, B., Kozlov, D. N., and Stempanoni-Pananriello, A., "Measurement of Gas Jet Flow Velocities Using Laser-Induced Electrostrictive Gratings," 18th European Coherent Anti-Stokes Raman Spectroscopy Workshop, March 1999.

[12]Schlamp, S., Cummings, E. B., and Sobota, T. H., "Laser-Induced Thermal-Acoustic Velocimetry with Heterodyne Detection," *Optics Letters*, Vol. 25, No. 4, 2000, pp. 224–227.

[13]Boyd, R. W., *Nonlinear Optics*, Academic Press, Boston, 1996, pp. 327–331.

[14]Yariv, A., *Optical Electronics*, 3rd ed., Holt, Rinehart, and Winston, New York, 1985, pp. 327–335.

[15]Stevens, B., *Collisional Activation in Gases*, Pergamon, Oxford, 1967, pp. 45–76.

[16]Pierce, A. D., *Acoustics, An Introduction to Its Physical Principles and Applications*, Acoustical Society of America, Woodbury, NY, 1981, pp. 547–560.

[17]Morse, P. M., and Ingard, K. U., *Theoretical Acoustics*, Princeton Univ. Press, Princeton, NJ, 1986, pp. 270–300.

[18]Bhatia, A. B., *Ultrasonic Absorption*, Dover, New York, 1985, pp. 71–167.

[19]Reid, R. C., Prausnitz, J. M., and Poling, B., *The Properties of Gases and Liquids*, McGraw–Hill, New York, 1987, pp. 388–432 and 514–530.

[20]Herzfeld, K. F., and Litovitz, T. A., *Absorption and Dispersion of Ultrasonic Waves*, Academic Press, New York, 1959, p. 239.

W. R. Lempert
Guest Associate Editor